JOURNAL OF CATALYSIS 141, 688–699 (1993)

The Effect of Redox Treatment on the Structural, Adsorptive, and Catalytic Properties of Raney Nickel

S. D. MIKHAILENKO, T. A. KHODAREVA, E. V. LEONGARDT, A. I. LYASHENKO, AND A. B. FASMAN

Institute of Organic Catalysis and Electrochemistry, 142 K. Marx St., 480100 Alma-Ata, Kazakhstan

Received August 10, 1992; revised January 28, 1993

The effect on Raney nickel catalyst of annealing in hydrogen, and of mild oxidation and subsequent reduction have been studied. The properties investigated are the structure, hydrogen adsorption, and activity for nitrobenzene and potassium maleate liquid-phase hydrogenation. Characterization involved X-ray line broadening, adsorption, and capillary condensation of Ar, XPS, and thermoprogrammed reduction. Thermodesorption studies indicate two forms of adsorbed hydrogen, one of which is a weakly bound molecular form and does not depend on treatment, while the other is strongly bound atomic hydrogen whose amount decreases with increase in the annealing temperature. Annealing in hydrogen at $T \geq 200°C$ causes sintering of the catalysts and a decrease in their activity. Mild oxidation leads to formation of a protective film from nonstoichiometric nickel–oxygen compounds on the Raney Ni surface, preventing it from deep oxidation in the air. A passivated catalyst can be reactivated by heating at 100–300°C in hydrogen, after which the activity for hydrogenation is on par with that of newly prepared catalyst.

INTRODUCTION

Interest in Raney nickel is caused on the one hand by its wide use in industrial organic synthesis and electrochemical energy conversion, and on the other hand by the complexity of this catalyst as an object of fundamental study. Much work has already been carried out by physical and physicochemical methods, and this has greatly contributed to the development of viewpoints on the mechanism of formation, structure, and physicochemical properties of Raney Ni. Among the most systematic and important works should be mentioned the series of the articles on the structure of Raney Ni published in 1969–1976 by Anderson and co-workers (*1–4*). An overview of publications prior to 1968 is given in Ref. (*5*). The results of later works are discussed in a review by Fouilloux (*6*). Traditional and modified Raney Ni are used mainly in hydrogenation and reduction reactions and, to a lesser extent, in hydrogenolysis. It is also used in various reactions in the absence of hydrogen in the gaseous phase and as an active phase of fuel cell electrodes (*7*). However, usage of Raney catalysts is often limited by their propensity for self-heating and self-ignition in the air. The nature of these phenomena is influenced by the high dispersion and strong lattice distortion of Raney Ni and by the presence of a large amount of hydrogen in an active form (*5*, *8–10*).

In order to obtain Raney catalysts stable for storage in the air, their surface should be protected from the deep and irreversible oxidation which causes a release of much heat. This can be achieved by protection of the surface by organic substances or by oxidation under mild conditions (*5*, *11*). A decrease in pyrophoric character can also be achieved by thermal treatment of the catalysts (*12*). The effect of thermal treatment on the structural, physicochemical, and adsorption properties of Raney catalysts was studied previously (*13–16*). It is shown that on annealing in reducing or inert media the number and character of surface defects, orientation of crystal faces, and the porous structure of Raney nickel change. With an increase in temperature of treatment, crystallite sizes also increase and the lattice

0021-9517/93 $5.00

constant changes, approaching the value typical for bulk nickel metal. Obviously, such a change of the structure affects catalyst properties.

The present work aims at studying the effect of thermal treatments in a redox medium on the structure and physicochemical properties of Raney nickel and at elucidation of its influence on adsorption characteristics and catalytic properties. Studies in this direction are expected to help in solution of the problem of production of Raney catalysts active and stable for storage.

EXPERIMENTAL

1. Preparation and Treatment of Catalysts

The starting alloy 50 wt% Ni–50 wt% Al was prepared in a high-frequency furnace (OKB-8020) in quartz crucibles and was subjected to a homogenizing annealing in Ar at 800°C. It was then crushed and dispersed in a vibrating grinder, and 60–100 μm fractions were isolated by sieving. Catalysts were prepared by leaching the starting alloy with 20% KOH solution in tenfold excess with respect to Al. Time of leaching was 2 h; temperature was 100°C. These conditions were chosen in order to obtain completely and uniformly leached samples, although sometimes leaching at a lower temperature results in more active catalysts, containing more hydrogen (*5–7*). After leaching, the catalysts were washed free from alkali and aluminates by distilled water. We call this kind of catalyst "fresh." Another kind used in the work was catalyst after treatment in hydrogen, oxygen, or argon, as shown in Table 1. The annealing of catalysts in hydrogen was carried out in a quartz cell placed in a programmed thermoblock, and the oxidation treatment was made in the same cell in O_2+Ar mixture. The oxygen feed was controlled by a device connected to a differential thermocouple which insured that the temperature of the samples during the oxidation did not exceed 30°C. Passivated catalysts 1o–4o were reduced at 150°C in hydrogen before being used in liquid-phase reaction of hydrogenation. Annealing in H_2 (catalysts 1–5) and reduction at 150°C (catalysts 1or–4or) had been carried out directly before using the catalysts. Fresh catalysts were kept in alcohol.

TABLE 1

Designation of Raney Ni Samples

Temperature of treatment in H_2 (°C)	Sample designation		
	Annealing in H_2	Oxidation after annealing	Reduction at 150°C after oxidation
100	1	1o	1or
200	2	2o	2or
300	3	3o	3or
400	4	4o	4or
500	5	—	—

2. Porous Structure and Specific Surface Area of Catalysts

These were determined by adsorption and capillary condensation of Ar at 77 K. Samples were transferred to an adsorption cell without contact with air. Wet fresh catalysts were dried at 70°C and 10^{-3} Pa for 4 h. The average pore radius, R, determined from the dV/dR vs R dependence, total porosity, V, and cumulative surface of pore walls, S_{cum}, were found by the numerical integration of the adsorption equation as in Ref. (*17*), similar to the Cranston–Inkley procedure (*18*). Micropores with $R < 15$ Å radius were not taken into account. Concurrently, the total catalyst surface area S_{BET} was calculated.

3. Crystallite Size (D) and Lattice Distortion

Calculations were made from the width of the X-ray diffraction lines for Ni(111) and Ni(222). Line profiles were recorded on a DRON-2.0 apparatus at the rate of 0.25 deg(2Θ)/min. Filtered Co K_α irradiation was used. The calculation was carried out by the method described elsewhere (*19*), assuming that the shape of X-ray lines is described by the Gauss function.

4. Composition of the Catalyst Surface

This was studied by X-ray photoelectron spectroscopy (XPS) using an ES-2402 (USSR) spectrometer and the method described in Ref. (20). Samples were pressed wet and dried in a spectrometer chamber at 10^{-4} Pa. The spectra showed that the main peak Ni $2p_{3/2}$ is always split into two components with 855.1 and 851.8 eV binding energies corresponding to Ni^{2+} and Ni^0 oxidation states. Al $2p$ XPS showed that aluminium is present on the surface as Al^{3+}. Atomic concentrations of the elements on the surface were estimated using the formula

$$[\mathrm{Me}_i] = I_i/\sigma_i \cdot \left[\sum_i I_i/\sigma_i\right]^{-1},$$

where I_i is the integral intensity of the respective line of the given metal and σ_i is the sensitivity factor. Oxygen (O $1s$) and carbon (C $1s$) spectra were also recorded.

5. Kinetics of Temperature-Programmed Reduction

A GDTD-24 (Setaram) apparatus was employed, with the sample placed on a filter made from sintered quartz powder in a U-shaped cell. The rate of gas flow (3–15% H_2 in Ar) was 0.8–1.0 cm^3 (STP)/s. The change of hydrogen concentration in the mixture was determined by a Cromadam gas chromatograph. Calculations of the kinetic parameters of reduction (k_0, the preexponential factor in the Arrhenius equation and E, the activation energy of reduction) are described in Appendix A.

6. Hydrogen Adsorption

The adsorption properties of the catalysts for hydrogen were studied by temperature-programmed desorption (TPD). Wet fresh catalysts were first dried in vacuum at 70°C and the adsorption was carried out at room temperature. For passivated catalysts the procedure was different. Hydrogen was adsorbed at 150–250°C during 1 h, and the sample was cooled to room temperature. In both cases the cell was then purged with argon and TPD measurements were started from room temperature at a heating rate $\beta = 0.16$ K/s.

The method used for calculation of the activation energy of hydrogen desorption (E_a) and the reaction order n (molecular adsorption at $n = 1$, dissociative adsorption at $n = 2$) is described in Appendix B.

7. Catalytic Properties

The activity of the catalysts was determined for the hydrogenation of substances with different adsorbability, namely, potassium maleate and nitrobenzene, which are weakly and strongly adsorbed on the catalyst surface, respectively (*21*, *22*). Nitrobenzene hydrogenation is also of practical interest, since it underlies the industrial process of aniline manufacture.

Hydrogenation was carried out in a batch reactor with vigorous enough mixing for the process to run in the liquid phase without diffusional limitation on the rate. This was implied, in particular, by a linear relationship between the reaction rate and the amount of catalyst.

Potassium maleate was hydrogenated in 0.1 *N* KOH, and nitrobenzene in 96% ethanol. The temperature of the experiments was 40°C. In the presentation and discussion of results, initial rates of the reactions at the moment of consumption of 5% hydrogen are compared.

RESULTS AND DISCUSSION

1. Thermal Treatment of Fresh Catalysts

Fresh catalysts were annealed for 1 hour in hydrogen at 100–500°C. They were heated to these temperatures at 10 K/min. Figs. 1–3 illustrate the change in crystallite size, lattice distortion, pore structure, and specific surface of Raney Ni as a function of temperature of annealing in hydrogen. From Figs. 1–3, it follows that annealing causes growth of crystallites and decrease in lattice distortion in the catalysts, catalyst porosity, and specific surface. S_{BET} starts to

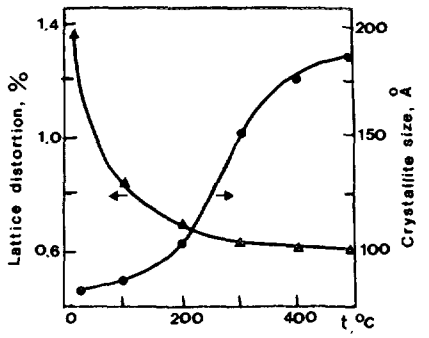

FIG. 1. Influence of temperature of Raney Ni annealing in hydrogen on its lattice distortion and crystallite size (D).

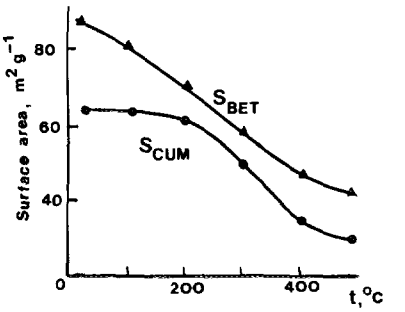

FIG. 3. Influence of temperature of Raney Ni annealing in hydrogen on its S_{BET} and S_{cum} surface area.

decrease before S_{cum} (Fig. 3), from which it follows that micropores, determined by the difference between S_{BET} and S_{cum}, are annihilated first.

On annealing, the average pore radius R grows. Heating of the catalyst above 400°C causes no appreciable change in its structure.

The decrease in hydrogenation activity on annealing is roughly proportional to the decrease in S_{BET}. Figure 4 illustrates the change in catalyst activity as a function of temperature and annealing time. Time of annealing τ was altered only in this experiment. At $\tau = 0$, a sample was heated to 50–500°C at 10 K/min and immediately removed from the furnace in a flow of hydrogen. It is interesting that at $\tau = 0$ the curve W vs t has a local minimum. Since the catalyst is charged wet into the cell, it is possible that this drop in the activity is caused by oxidation with water on heating to 100°C. An increase in the annealing time in hydrogen reduces the catalyst and restores its original activity. The same result is obtained on increasing the annealing temperature to 200–250°C despite the fact that S_{BET} is decreased by 10–30%. A further increase in the temperature causes a more substantial decrease in S_{BET} and catalyst activity. This in part can be explained by the fact that a decrease in surface area under these conditions occurs mainly at the expense of a decrease in the proportion of micropores from $\varphi = 0.25$ to $\varphi = 0.05$ ($\varphi =$

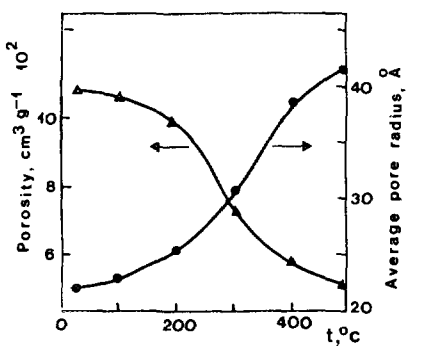

FIG. 2. Influence of temperature of Raney Ni annealing in hydrogen on volume V and mean radius of pores R.

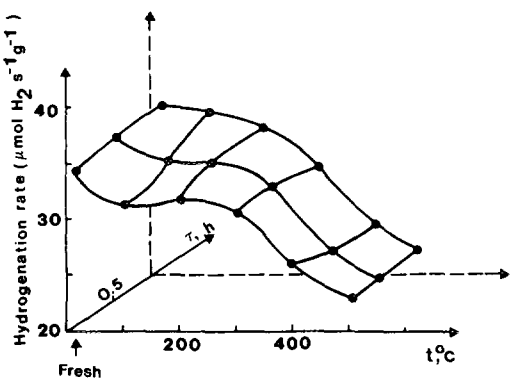

FIG. 4. Influence of temperature and time of Raney Ni annealing on its activity for nitrobenzene hydrogenation at 40°C.

($S_{BET} - S_{cum}$)/S_{BET}). As a result, the value of the pore radius R grows markedly, while on annealing above 200°C it decreases. Thus, sintering above 300°C does not change the activity of Raney Ni since it affects mainly that part of the pore space which is not apparently involved in the activation of reactants due to difficulties in diffusion in the pores. Owing to this, SCA (specific catalyst activity per unit surface) of samples 1–3 is increased by 1.5-fold. Diffusional limitations for Raney nickel, as shown in Ref. (*23*), exist when the size of catalyst particles is greater than 1–3 μm. For particles of 60–100 μm, as we have here, according to the estimates of Ref. (*23*), the rate of hydrogenation can be 30–50% of the maximal value.

XPS studies show that on annealing Raney Ni its surface becomes enriched with Al (Table 2). The binding energy (E_B) of the Al 2*p* peak occurs at E_B = 74.7 eV, which corresponds to an oxidation state of Al^{3+} for aluminium, indicating the presence of Al_2O_3. In alloys, either the components with the lowest sublimation heat or those most actively interacting with the reaction medium are known to segregate to the surface (*24*, *25*). These factors can hardly account for the increase in the Al_2O_3 proportion on the surface of Raney Ni. Most likely, this increase is caused by sintering of metal particles leading to a decrease in the metal proportion on the surface, if it is remembered that Al_2O_3 surface value is not altered at such temperatures.

The content of oxidized nickel in the catalyst surface layers is unchanged by thermal treatment (Table 2). It may be that slight oxidation occurs on the drying of a wet sample in the apparatus chamber.

TABLE 2

Influence of Thermal Treatment in H_2 on Composition of Raney Ni Surface

Surface composition	Catalyst			
	Fresh	1	3	5
Ni/(Ni + Al)	0.90	0.92	0.70	0.35
$Ni^0/(Ni^0 + Ni^{2+})$	0.93	0.96	0.90	0.92

The number of defects in the catalysts does not affect markedly their activity in nitrobenzene hydrogenation. From the comparison of Figs. 1 and 4 it can be seen that annealing at 100–200°C causes a sharp decrease in lattice distortion, i.e., in the number of defects in the catalysts, while the activity remains unaffected. The same result was obtained for hydrogenation of potassium maleate.

Thus, the catalytic properties of Raney Ni annealed in H_2 are determined by sintering which causes a decrease in the active surface area on the one hand, and a decrease in diffusion difficulties when transporting reactants, and an increase in SCA (specific catalyst activity), on the other hand.

2. *Mild Oxidation of Catalysts*

Catalysts annealed in hydrogen retain their pyrophoric properties but can be stabilized by means of slow oxidation in a low partial pressure of oxygen (*26*, *27*). By oxidative treatment of samples 1–4 in Ar + O_2 mixture, we have obtained powders stable for storage in the air. Table 3 lists the data on crystallite size, lattice distortion, surface composition, and surface area. It can be seen that the surface area of the pores with $R > 15$ Å (S_{cum}) in all the oxidized catalysts (1o–4o) is very similar. The total surface area (S_{BET}) is decreased from 38 in sample 1o to 32 m^2/g in sample 4o, while the proportion of micropores in the latter is 20% less.

The dispersion of samples 3 and 4 is not altered after oxidation, while in samples 1 and 2, *D* is increased to 120–140 Å. Judging by the *D* vs *T* relation (Fig. 1), it can be assumed that the local heating of catalyst particles in oxidation is only 200–300°C.

One can note an increase in the lattice distortion in Raney Ni particles after oxidation. This may be due to penetration of oxy-

TABLE 3

Influence of Annealing Temperature on Specific Surface Area (S), Crystallite Size (D), Lattice Distortion, and Surface Composition of Raney Ni after Annealing in Hydrogen (1–4), Oxidation (1o–4o), and Reduction at 150°C in Hydrogen (1or–4or)

Sample	1	1o	1or	2	2o	2or	3	3o	3or	4	4o	4or
S (m^2/g)												
S_{BET}	82	38	58	73	35	49	60	34	49	48	32	49
S_{cum}	62	28	49	61	28	30	60	34	49	48	32	49
D(Å)	60	120	130	100	140	160	150	150	175	180	180	175
Lattice distortion (%)	0.85	1.0	0.72	0.70	0.81	0.72	0.65	0.82	0.72	0.60	0.78	0.68
Surface comp.[a]												
Ni/(Ni + Al)	0.92	0.41	0.48	—	0.36	0.45	0.70	0.28	0.41	—	0.26	0.29
$Ni^0/(Ni^{2+} + Ni^0)$	0.96	0	0.29	—	0	0.33	0.90	0.17	0.38	—	0.17	0.44
Oxygen/(Ni + Al)	0.6	1.1	0.7	—	1.0	0.6	0.6	1.0	0.6	—	0.8	0.6

[a] Surface composition from XPS.

gen into the metal lattice. In this case, the greatest distortions of the lattice may be expected to occur in samples having maximal S_{BET} before oxidation, which is in fact observed.

According to the XPS data (Table 3), the amount of Ni on the oxidized catalysts decreases with a change of the annealing temperature from 100 to 400C°. The content of zero-valent metal on Raney Ni surface after oxidation is not high, while that of oxygen according to the O 1s peak approaches 50%. Thus, as follows from the data on adsorption and capillary condensation of Ar, the oxidation treatment makes the pore structure parameters of catalysts 1–4 more close, whereas the chemical composition of their surfaces is very different.

The study of the oxygen-containing components of the Raney Ni surface was carried out by the TPR method. Figure 5 presents TPR spectra, while Table 4 gives the volume of hydrogen consumed, the temperature of consumption maxima, the activation energy of reduction, and the total

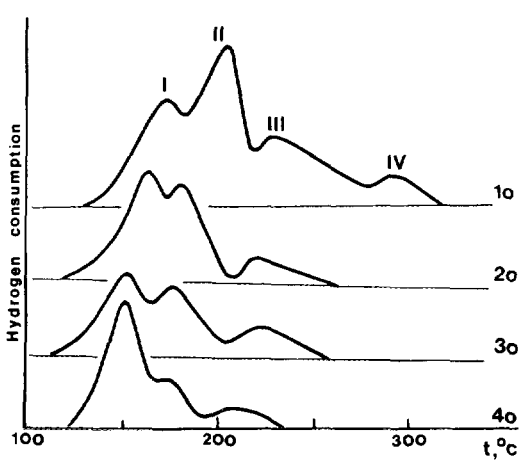

FIG. 5. TPR spectra of Raney Ni, prepared under different conditions.

TABLE 4

Influence of Conditions of Raney Ni Treatment on TPR Parameters

	Sample			
	1o	2o	3o	4o
Consumption H_2 (cm^3/g)	25.0	12.0	9.6	8.5
Peak I				
T_{max}(°C)	176	167	152	146
$p + q$	1.3	1.2	1.1	1.1
E(kJ/mol)	114	112	107	105
Peak II				
T_{max}(°C)	201	180	174	170
$p + q$	1.2	1.1	1.0	1.0
E(kJ/mol)	126	123	120	119
Peak III				
T_{max}(°C)	226	211	211	208
$p + q$	1.1	1.1	1.0	1.0
E(kJ/mol)	137	136	135	135
Peak IV				
T_{max}(°C)	288	—	—	—
$p + q$	1.0	—	—	—
E(kJ/mol)	179	—	—	—

reaction order for hydrogen, and reducible substance $p + q$. Samples 1o–4o differ appreciably both in the content of reducible phases and their energy characteristics. It is found (*28*) that reduction of bulk NiO proceeds within the 290–320°C range. Apparently, peak IV in the TPR spectrum (Fig. 5) displays the reduction of NiO films partially covering, as mentioned earlier (*29*), Raney Ni granules. The presence of maxima I–III at lower temperatures confirms the hypothesis advanced earlier (*30*) about the presence of nonstoichiometric nickel–oxygen structures on the surface of such catalysts. These structures differ little in their reduction activation energies, and their TPR maxima are separated by intervals of approximately 50°C.

It is most interesting that with a growth in temperature of pretreatment in hydrogen the content of the more stable oxides sharply decreases, mainly at the expense of maxima II and III. The most labile form, to which peak I corresponds, is preserved in all the samples, while the activation energy of its reduction decreases with an increase in the annealing temperature. The more the content of the other oxide forms decreases, the higher is the activation energy of their reduction. In each case, the total reaction order is close to unity.

Thus, a high-proportion of the surface oxide components consist of nonstoichiometric compounds of nickel with oxygen possessing a high energy barrier of reduction. Protecting Raney Ni from self-ignition and deep oxidation in the air, they simultaneously make it inactive in liquid-phase hydrogenation reactions.

3. Reactivation of Passivated Catalysts

The presence on the surface of catalysts 1o–4o of mainly nonstoichiometric compounds of nickel with oxygen makes their reactivation possible even under mild conditions, as shown in Ref. (*31*). Figure 6 presents the dependence of activity of samples 1o–4o on reduction temperature. Optimal conditions of reactivation of all the catalysts are within the 200–250°C range. A decrease in the activity at higher temperatures is caused, apparently, by their sintering. As after the reduction at 200–250°C the activity of samples 1or and 2or differs little, the structure and adsorption properties of catalysts were compared after the reduction at 150°C when hydrogenation rates are clearly different.

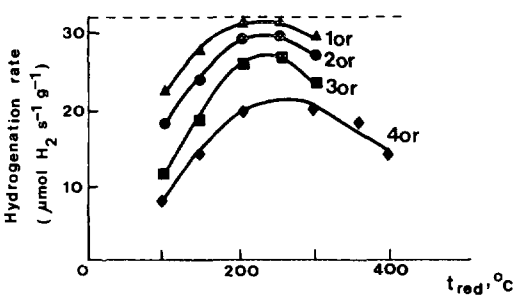

FIG. 6. Influence of reduction temperature on activity of passivated catalysts for nitrobenzene hydrogenation at 40°C; (- - - -) activity of fresh catalyst.

From Table 3 it follows that samples 2or–4or have almost equal surface areas of S_{BET} and S_{cum}, whereas 1or is markedly more dispersed and possesses a more developed surface. The reduction levels the difference in the catalyst lattice distortion, while the proportion of zero-valent nickel on the surface is increased with the temperature of annealing in hydrogen.

Adsorption properties of the catalysts for hydrogen were studied by TPD (Fig. 7, Table 5). Irrespective of treatment, the samples have two forms of adsorbed hydrogen. The first is weakly bound and molecular (reaction order $n = 1$), and is desorbed with a maximum at 110–118°C. The second is a strongly bound dissociative form (reaction order $n = 2$) whose T_{max} of desorption varies over a wider range, from 163 to 196°C. In addition, all the reduced catalysts have a high-temperature peak III which characterizes an atomic form of adsorption ($n = 2$) and a high activation energy of hydrogen desorption. Redox treatment causes a redistribution of the energy inhomogeneity of the surface. With an increase in the annealing temperature in hydrogen, desorption peaks are shifted to a lower temperature, and the total amount of hydrogen desorbed decreases from 23.7 for the starting catalyst to 7.2 cm^3/g for sample 4or. This is evi-

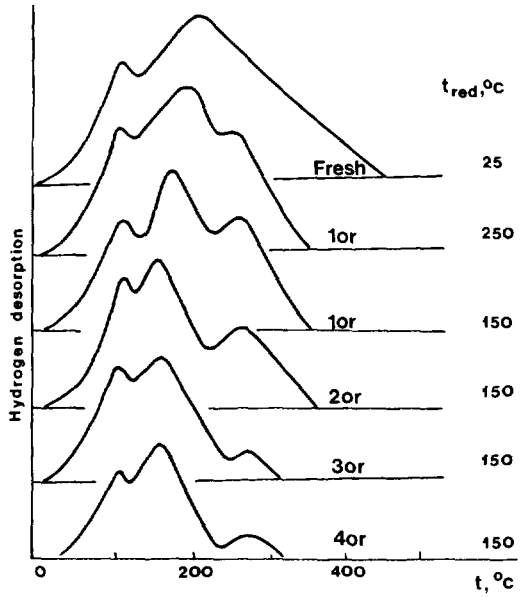

FIG. 7. TPD spectra of reduced Ni subjected to treatment under different conditions.

TABLE 5

Influence of Preparation Conditions on the Hydrogen Adsorption Properties of Raney Ni

Sample	Fresh	1o		2o	3o	4o
$T_{red.}$ (°C)	25	150	250	150	150	150
Total amount of H_2 desorbed (cm^3/g)	23.2	13.9	14.4	13.4	10.9	7.2
Peak I						
T_{max}(°C)	118	114	114	112	110	110
n	1	1	—	1	1	1
E(kJ/mol)	42.1	39.9	—	41.4	39.5	36.6
Amount (cm^3/g)	4.8	3.6	3.8	3.8	3.9	2.7
Peak II						
T_{max}(°C)	196	176	191	162	162	163
n	2	2	—	2	2	2
E(kJ/mol)	73	69	—	62	61	57
Peak III						
T_{max}(°C)	—	262	265	262	258	258
n	—	2	—	2	2	2
E(kJ/mol)	—	139	—	139	137	132

dently due to a decrease in S_{BET} (Fig. 3). A decrease in the lattice distortion of the respective samples leads to a decrease in the amount of hydrogen adsorbed, mainly at the expense of a strongly bound form.

The change in the adsorption characteristics of the catalysts may be expected to affect their catalytic activity. In fact, the rate of nitrobenzene reduction correlates with the content of strongly bound hydrogen. Figure 8 illustrates the change of catalyst activity and the amounts of weakly and strongly bound hydrogen as a function of the annealing temperature, whence it can be seen that the decrease in the rate of nitrobenzene hydrogenation is proportional to the decrease in the content of strongly bound hydrogen, whereas the amount of the weakly bound form is only slightly altered on annealing. This agrees with data reported, for instance, in Ref. (*21*), where it is shown that the absence of strongly bound hydrogen leads to irreversible adsorption of nitrobenzene and poisoning of the catalyst. However, the hydrogenation rate of potassium maleate, which can be reduced by weakly bound hydrogen, does not depend on the conditions of Raney Ni pretreatment and does not differ from that typical for the

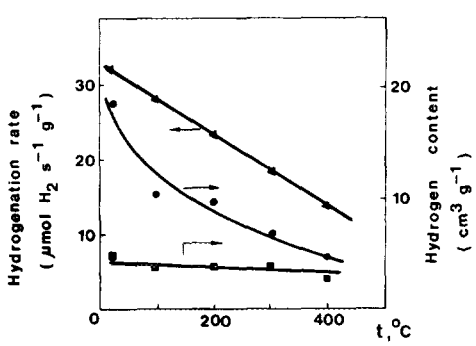

FIG. 8. Influence of temperature of Raney Ni annealing in hydrogen on the contents of weakly and strongly bound hydrogen and on the activity of catalysts passivated and reduced at 150°C for nitrobenzene hydrogenation at 40°C: ▲, hydrogenation rate; ■, amount of weakly bound hydrogen; and ●, amount of strongly bound hydrogen.

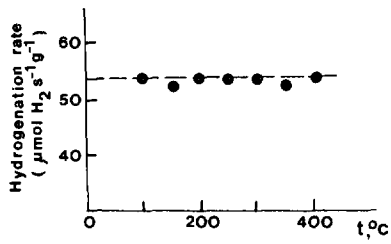

FIG. 9. Influence of annealing temperature on activity of Raney Ni passivated and reduced at 150°C for potassium maleate hydrogenation at 40°C; (- - - -) activity of fresh catalyst.

starting sample (Fig. 9). The increase in temperature of reduction up to 250°C alters the adsorption properties of the catalyst in the direction of an increase in the content of strongly adsorbed hydrogen. The shape of the TPD profile approaches that typical for a fresh catalyst, and the rate of nitrobenzene hydrogenation of the catalyst reduced at 250°C is the same as that of the fresh one (Fig. 6).

From Table 3 it can be seen that reduction of the catalysts leads to an increase in S_{BET}, while S_{cum} is increased only for sample 1or. During reduction, this catalyst takes up the highest amount of hydrogen, and its TPR profile points to the greatest diversity of nickel–oxygen structures. It can be assumed that reactivation leads to partial reduction of the active catalyst surface blocked during passivation by oxides on the one hand, and to formation of a new active form from nickel microcrystals by reduction of nonstoichiometric oxides, on the other. Coarser catalyst particles serve as a support for this new structural component which can be called "surface nickel black." The scheme in Fig. 10 illustrates processes of sintering, oxidation and reduction of Raney Ni. The highest amount of "nickel black" is expected to form during reduction of sample 1o which, according to TPR data, takes up three times more hydrogen than sample 4o. This accounts for its maximal activity for nitrobenzene hydrogenation.

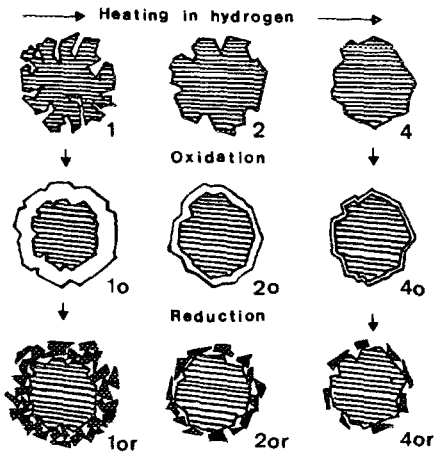

FIG. 10. Scheme of Raney Ni transformation during annealing (samples 1,2,4), oxidation (1o,2o,4o), and reduction (1or,2or,4or).

CONCLUSIONS

Thermal treatment in a reduction medium leads to sintering of Raney Ni with a concurrent decrease in its lattice distortion and increase in crystallite size. With an increase in annealing temperature the free energy of the catalyst surface decreases, and as a result a lower amount of heat is released and the oxidation depth is decreased on their stabilization by mild oxidation. The protecting oxide film is easily reduced under mild conditions to form a layer of highly dispersed "surface Ni black." The amount of the new active form is proportional to the content of nonstoichiometric metal–oxygen compounds on the surface of stabilized Raney Ni and decreases with increase in the temperature of preannealing. On reduction, transformation of the oxygen-containing films to microcrystals results in a partial release of formerly covered catalyst surface causing a growth in S_{BET}. The reduced catalyst is capable of adsorbing more than 60% of hydrogen compared with a fresh one, and is on par with the latter in terms of activity for hydrogenation of potassium maleate and nitrobenzene.

Hence, by thermal treatment in reducing and oxidizing conditions, one can not only increase substantially the stability of Raney Ni to storage in the air, but one can also control its structure, composition, surface morphology, and adsorption characteristics and thereby affect its catalytic properties.

APPENDIX A

Calculation of Kinetic Parameters of Temperature-Programmed Reduction

As in Refs. (*28*, *32*) calculations of k_0 and E were based on the equation

$$-\frac{d\Omega}{dt} = \mu \frac{dn}{dt} = k_0 \cdot \Omega^q \cdot n^p \cdot \exp(-E/RT), \quad (1)$$

where Ω is the amount of reducible substance reduced at time t, and n is the number of moles of hydrogen consumed in the same time, μ is the stoichiometric coefficients, k_0 the preexponential factor in the Arrhenius equation, q and p are the reaction orders for the reducible substance and hydrogen, and E is the activation energy of reduction. Since $\Omega = \mu \cdot n$, for the linear heating at $\beta = dT/dt$ rate one obtains

$$\frac{dn}{dt} = \frac{k_0}{\beta} \cdot \mu^{q-1} \cdot n^{q+p} \cdot \exp(-E/RT), \quad (2)$$

and taking logarithms

$$\ln\left[\frac{dn/dt}{n^{q+p}}\right] = \frac{k_0 \cdot \mu^{q-1}}{\beta} - \frac{E}{R} \cdot \frac{1}{T}. \quad (3)$$

From the experimental curve $dn/dT = f(T)$, we found values f_i for various T in particular regions of peaks in order to obtain data to plot Eq. (3). Kinetic parameters of k_0 and E were calculated by the least-squares method. The total reaction order $p + q$ was varied within the 0–2 range by 0.1 steps. Also calculated was the mean-square error

$$V_x = \left[\left[\sum_i^m (f_i - \bar{f})^{-2}\right] \cdot (m-1)^{-1}\right]^{1/2} \cdot m \cdot \left(\sum_i^m f_i\right)^{-1},$$

where m is the number of values f_i. The solution with $(q + p)$ was chosen for which V_x was the lowest.

Most difficult in the calculation by the above method is the correct deconvolution of peaks. However, in these experiments calculations show the solutions of Eq. (3) to be stable enough to the method of processing of the data. Several variants of deconvolutions of TPR spectra lead to E values differing from each other by not more than 20%. In order to check the calculation method, another way of obtaining k_0 and E was used based on the dependence of the maxima of the TPR curve on the rate of heating β, as in Ref. (*33*). For one of the samples an experiment was carried out at $\beta = 0.08$, 0.16, 0.28, and 0.33 K/s, and the values of E obtained differed by no more than 20%. In all other cases $\beta = 0.16$ K/s, and we used the method of calculation for E and k_0 described above.

APPENDIX B

Calculation of Kinetic Parameters of the Temperature-Programmed Desorption

E_a and n were calculated from the equation

$$\frac{d\Theta}{dT} = \frac{\Theta^n}{\beta} \cdot k_0 \cdot \exp(-E_a/RT), \qquad (4)$$

where Θ is the surface coverage by hydrogen; $n = 1$ or 2 is the reaction order (molecular adsorption at $n = 1$; dissociative adsorption at $n = 2$) and E_a is the activation energy of hydrogen desorption. Integrating and taking logarithm of Eq. (4), one obtains for $n = 1$,

$$\ln\left(-\ln\frac{\Theta}{T^2}\right) = A - \frac{E_a}{R} \cdot \frac{1}{T}, \qquad (5)$$

and for $n = 2$,

$$\ln\left(\frac{1-\Theta}{\Theta \cdot T^2}\right) = A - \frac{E_a}{R} \cdot \frac{1}{T}, \qquad (6)$$

where A is a constant. E_a for Eqs. (5) and (6) was calculated by the least-squares method. Selection of the solution was made from a minimal V_x error.

REFERENCES

1. Freel, J., Pieters, W. J. M., and Anderson, R. B., *J. Catal.* **14,** 247 (1969); **16,** 281 (1970).
2. Freel, J., Robertson, S. D., and Anderson, R. B., *J. Catal.* **18,** 243 (1970); **24,** 130 (1972).
3. Robertson, S. D., and Anderson, R. B., *J. Catal.* **23,** 286 (1971); **41,** 409 (1976).
4. Macnab, J. I., and Anderson, R. B., *J. Catal.* **29,** 328 (1973); **29,** 338 (1973).
5. Fasman, A. B., and Sokolskii, D. V., "Structure and Physicochemical Properties of Raney Catalyst." Nauka, Alma-Ata, 1968.
6. Fouilloux, P., *Appl. Catal.* **8,** 1 (1983).
7. Gildebrand, E. I., and Fasman, A. B., "Raney Catalysts in Organic Chemistry." Nauka, Alma-Ata, 1982.
8. Bekassy, S., and Petró, J., *Thermochim. Acta.* **11,** 45 (1975).
9. Tungler, A., Bekassy, S., and Petró, J., *Acta Chim. Acad. Sci. Hung.* **86,** 347 (1975).
10. Bekassy, S., Petró, J., Kristyak, E., Csanady, A., and Kalman, A. *Acta Chim. Acad. Sci. Hung.* **88,** 375 (1976).
11. Chesnokova, R. V., Bykov, B. G., Bondareva, A. A., Sushkova, L. A., Alekseev, A. M., Vasilevich, A. I., and Sazonova, I. S., *Kinet. Katal.* **25,** 207 (1984).
12. Leongard, E. V., Mikhailenko, S. D., Lyashenko, A. I., and Fasman, A. B., *Zh. Fiz. Khim.* **60,** 323 (1986).
13. Nakabayashi, I., *Nippon Kagaku Zasshi* **90,** 344 (1969).
14. Hofer, E. M., and Hintermann, H. E., *Microtechnic* **20,** 183 (1966).
15. Erzhanova, M. S., Sokolskii, D. V., Popov, N. I., and Kondratenko, V. I., *Zh. Fiz. Khim.* **51,** 424 (1977); **51,** 884 (1977).
16. Baird, T., Paál, Z., and Thomson, S. J., *J. Chem. Soc. Faraday Trans. I* **69,** 50 (1973); **69,** 1241 (1973).
17. Mikhailenko, S. D., Fasman, A. B., Maksimova, N. A., Leongard, E. V., Antoshin, G. V., and Shpiro, E. S., *Appl. Catal.* **12,** 141 (1984).
18. Cranston, R. W., and Inkley, F. A., *Adv. Catal.* **9,** 143 (1957).
19. Gallezot, P., *in* "Catalysis Science and Technology" (J. R. Anderson and M. Boudart, Eds.), 5, p. 221. Springer, Berlin, 1984.
20. Minachev, Kh. M., Antoshin, G. V., and Shpiro, E. S., "Photoelectron Spectroscopy and Its Application to Catalysts." Nauka, Moscow, 1981.
21. Sokolskii, D. V., "Hydrogenation in Solutions." Nauka, Alma-Ata, 1979.

22. Shmonina, V. P., and Abdrakhmanova, R. M., *Zh. Obshch. Khim.* **34,** 869 (1964).
23. Safronov, V. M., Vorob'eva, V. I., and Fasman, A. B., *Zh. Prikl. Khim.* **57,** 1335 (1984).
24. Sachtler, W. M. H., and van Santen, R. A., *Adv. Catal.* **26,** 69 (1977).
25. Menon, P. G., and Prasada Rao, T. S. R., *Catal. Rev.-Sci. Eng.* **20,** 97 (1979).
26. Patent France No. 1595642 (17.07.1970).
27. Patent Japan No. 46-21363 (17.06.1971).
28. Monti, D. A. M., and Baiker, A., *J. Catal.* **83,** 323 (1983).
29. Mikhailenko, S. D., Khlystov, A. S., Maksimova, N. A., and Fasman, A. B., *React. Kinet. Catal. Lett.* **23,** 25 (1983).
30. Fasman, A. B., Leongard, E. V., Vishnevetskii, E. A., Lyashenko, A. I., and Mikhailenko, S. D., *Zh. Fiz. Khim.* **56,** 1269 (1983).
31. Slinkin, A. A., Kucherov, A. V., Fedorovskaya, E. A., and Rubinstein, A. M., *Kinet. Katal.* **28,** 742 (1977).
32. Hurst, N. W., Gentry, S. J., Jones, A., McNicol, B. D., *Catal. Rev.-Sci. Eng.* **24,** 233 (1982).
33. Sklyarov, A. V., *Usp. Khim.* **55,** 450 (1986).